COBEM 2021 26th International Congress of Mechanical Engineering
November 22-26, 2021, Virtual Congress, Brazil

COB-2021-1222
EXPERIMENTAL INVESTIGATION ABOUT EDISON TYPE THERMOMAGNETIC MOTORS BEHAVIOR OPERATING WITH A SMALL TEMPERATURE GRADIENT

Carlos Vinicius Xavier Bessa
João de Sá Brasil Lima
Bruno Chieregatti
Instituto Mauá de Tencologia – IMT – Praça Mauá, 1, São Caertano do Sul – SP,09580-900, Brasil
e-mails carlos.bessa@maua.br, joao.brasil@maua.br, bruno.chieregatti@maua.br

Ricardo Alexandre Galdino da Silva
Universidade Federal de São Paulo – UNIFESP – Rua Manoel da Nóbrega, 1535, Diadema – SP, 09910-720, Brasil
e-mail galdino.ricardo@unifesp.br

Lucas Diego Rodrigues Ferreira
Universidade São Judas Tadeu – Av. Vital Brasil, 1000, Butantã, São Paulo – SP, 05503-001, Brasil
e-mail lucas.ferreira@saojudas.br

Abstract. *Thermomagnetic motors are thermal engines that present the potential to obtain mechanical power from a small temperature gradient, with a high efficiency related with the Carnot efficiency. These devices are a promising technology for heat waste recovery and energy harvesting from vertical ocean temperature gradients, geothermal and solar sources. This study presents an experimental approach to investigate an Edison-type thermomagnetic motor operating around room temperature. The studied thermomagnetic motor uses pure gadolinium as a thermomagnetic rotor. A magnetic circuit using a NdFeB permanent magnet provides the applied magnetic field from 0 up to 0.85 T. The prototype relationships between output mechanical power and shaft angular velocity were obtained for heat sink and source temperatures from 283 K to 308 K and the different torque applied to the motor shaft conditions. The highest angular velocity, 0.8 rad/s, was found for the heat sink at 288 K and the heat source at 308 K with no torque applied to the motor shaft. The highest output mechanical power, 12 mW, was obtained for the same temperature condition with a motor's shaft applied torque of 0.02 N.m. The results show that these devices can produce mechanical power from temperature gradients lower than 10 K. The prototype developed in this study can contribute to a greater theoretical understanding of thermomagnetic motors in general, which could be a relevant energy harvesting device in diverse applications in the near future.*

Keywords: *thermomagnetic motors, energy harvesting, heat waste recovery*

1. INTRODUCTION

The increase in the global energy demand, associated with the need to reduce greenhouse gas emissions caused by the burning of fossil fuels, make the use of renewable sources and better energy use essential (Ahmed et al., 2021; Lima et al., 2020; Mehmood et al., 2021). Thermomagnetic motors are devices capable of converting heat into mechanical power through the thermomagnetic effect, i.e., the influence of the temperature on the magnetic material magnetization, presenting a high second order efficiency for small temperature gradients (Bessa et al., 2018). These devices are a promising technology for better energy use and have already been proposed for large-scale power generation (Egolf et al., 2009; Vuarnoz et al., 2012) and ultra-low power requirement applications (Kohl et al., 2018). Moreover, these machines can operate using low-quality heat waste (Almanza et al., 2017; Kaneko et al., 2020; Kishore et al., 2020; Lima et al., 2020), solar energy (Alves et al., 2013; Ferreira et al., 2014), vertical ocean temperature gradient, geothermal, and other sustainable thermal sources.

According to their architecture, thermomagnetic motors can be classified as Tesla type, based on Nikola Tesla patent (Tesla, 1889), or Edison type, based on Thomas Edison patent (Edison, 1888). At the first one, the heat transfer and work performance processes occur at different time intervals, simplifying the device operation and thermodynamic cycle analysis (Bessa, 2018). On the other hand, in the Edison type thermomagnetic motors, heat transfer and work are carried out simultaneously, making the thermodynamic cycle, heat transfer, and device dynamics analysis complex (Ferreira, 2019).

This study presents a prototype and an experimental investigation about Edison type thermomagnetic motors' behavior. The results obtained can be used to validate mathematical models and to a better understanding of this technology, contributing to the development of this technology and its applications in the use of thermal waste and other renewable energy sources.

2. THE EDISON TYPE THERMOMAGNETIC MOTOR

The Edison type thermomagnetic motor, also known as Currie wheel (Karle, 2001), consists of two main parts: a stator that provides the applied magnetic field to the machine; and a magnetic material (MM) rotor subjected to a temperature gradient around its Curie temperature (T_C), i.e., the temperature at which the MM undergoes magnetic transition, changing from a ferromagnetic to a paramagnetic state during a heating process our vice-versa during a cooling process.

Figure 1a shows a representation of an Edison type thermomagnetic motor. The MM rotor is heated by the heat source, at temperature T_{Hot}, placed next to the stator, where permanent magnets provide an applied magnetic field (H) gradient. The heat transfer causes a temperature gradient around the MM T_C, the material portion with temperature higher than Tc becomes paramagnetic, having a drastic reduction in its magnetization (M). The material portion that has temperature below Tc is ferromagnetic, having a high magnetization. The magnetic force is directly proportional to M (Gama et al., 2016), in this way, the temperature gradient causes an unbalance of forces in the MM rotor, where the magnetic force in the paramagnetic material portion (F_p) is lower than the magnetic force in it ferromagnetic portion (F_m), as shown in Figure 1b. This force imbalance results in a magnetic torque applied to the rotor, making the rotor turn with an angular velocity (ω). For a continuous operation, it is necessary to reject heat to the heat sink at temperature T_{Cold}, which characterizes these machines as thermal motors.

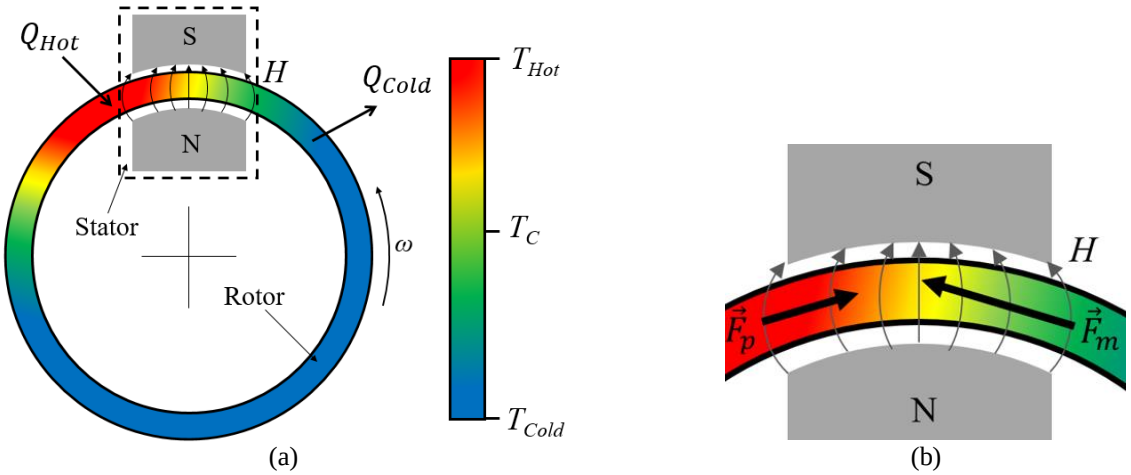

Figure 1. (a) Schematic view of an Edison type thermomagnetic motor. (b) Unbalance magnetic forces on the rotor.

3. DEVELOPED PROTOTYPE

In order to better understand the behavior of Edison type thermomagnetic motors, a prototype of it was developed for experimental investigation. The prototype parts and assembly are described below.

3.1 Stator Magnetic circuit

Figure 2 shows the magnetic circuit that provides the applied magnetic field to the prototype. It consists of a NdFeB 50M block with 50x50x100 mm³ permanent magnet associated with a field concentrator made of SAE1020 steel (soft magnetic material) that intensifies the magnetic field in the gap region. This simple arrangement can provide a high magnetic field, however, it uses a large permanent magnet and a considerable amount of steel, significantly increasing the weight of the system. The stator has a mass of around 6,65 kg. It is possible to get high magnetic fields using more complex and lighter magnet arrays, for instance, a Halbach array (Halbach, 1980). However, as the objective of this prototype is to be a platform for experimental tests, we did not seek to minimize the total motor weight, opting for a simple magnetic circuit using a single permanent magnet block.

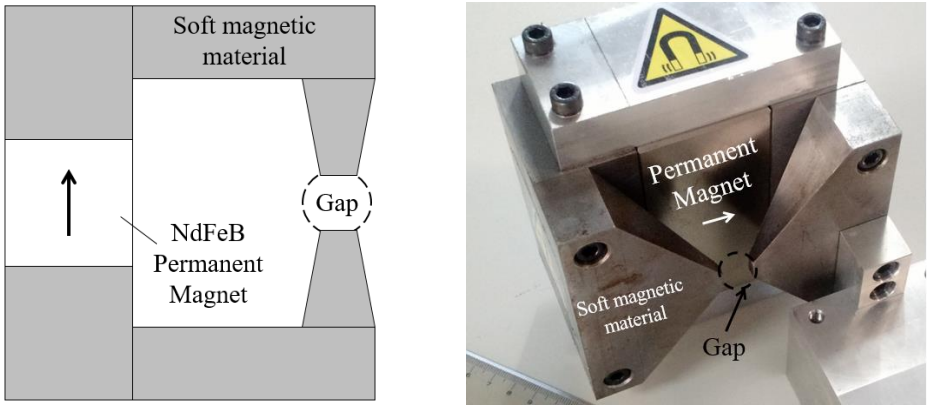

Figure 2. Prototype stator that provides the applied magnetic field.

3.2 Thermomagnetic rotor

Gadolinium (Gd) was used as the rotor magnetic material; it has well-known thermomagnetic properties and a *Tc* of 293 K, near room temperature, making it an excellent reference material (Risser et al., 2012). In addition, it can be rolled, formed, and machined. Figure 3 shows the MM rotor and some intermediate stages for obtaining it. Figure 3a shows the ingot obtained using 99,99% pure Gd by arc melting and homogenized using the procedure described by Paganotti (Paganotti et al., 2019). After that, an electric furnace heated the ingot to 973 K, and it was subjected to a roll forming process, obtaining a long Gd strip, which was formed into a ring, as shown in Figure 3b. Next, the ring was machined, obtaining a regular geometry with Ø96xØ93x10 mm³ and 32.3217 g, as shown in Figure 3c. Finally, the Gd ring was glued to a Celeron disc to support it. An N-type thermocouple was placed between the Gd ring and the Celeron disk, allowing the temperature determination at a rotor point during the tests, as shown in Figure 3d.

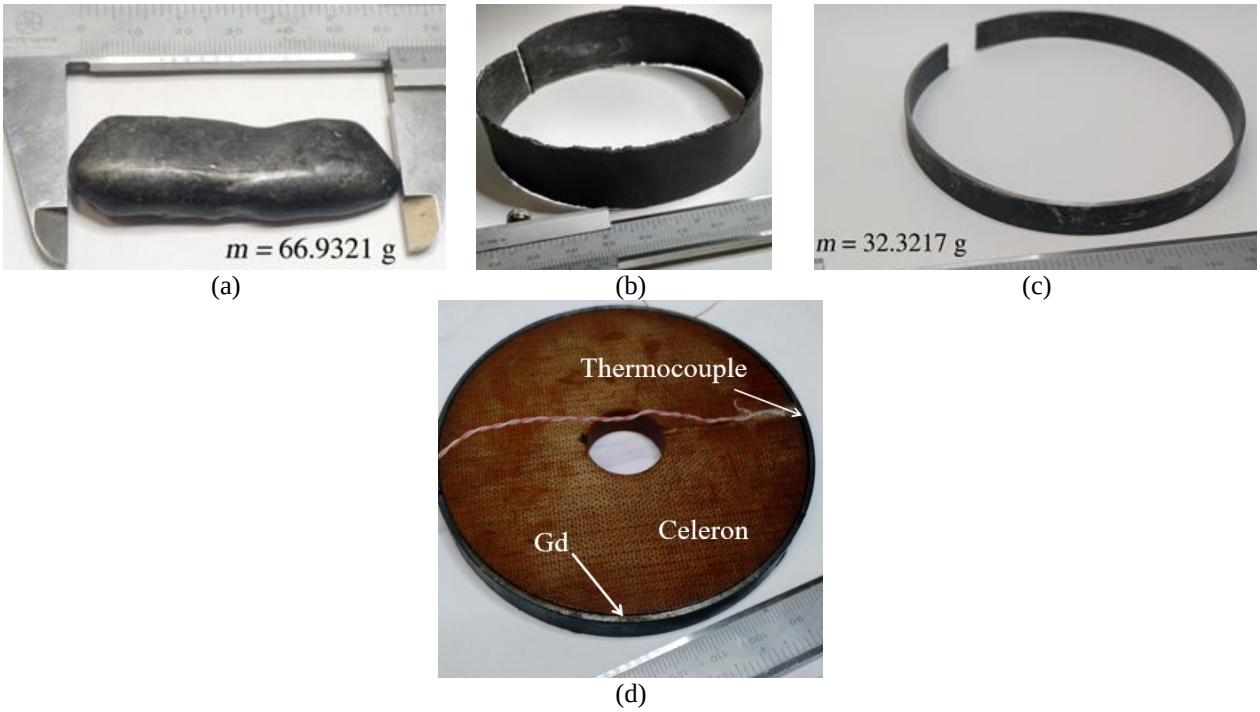

Figure 3. Prototype Gd rotor.

3.3 Assembled Prototype

Figure 4a shows the prototype. The Gd rotor was placed on an aluminum shaft supported by two block bearings, a flexible jaw shaft coupling the shaft to an angular encoder. The shaft features a pulley for load application and a slip ring to connect the thermocouple rotor to the acquisition data system. The stator magnetic circuit was attached to the

same aluminum support where the block bearings are fixed. Figure 4b shows the Gd rotor placed in the 12 mm gap region.

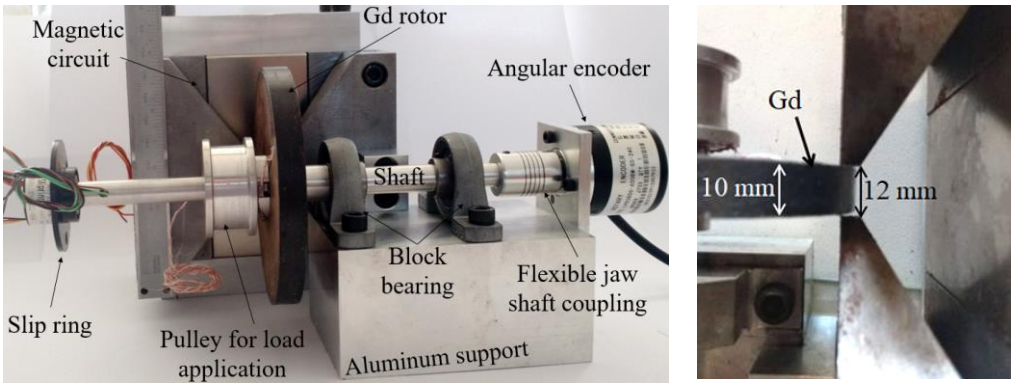

(a) (b)

Figure 4. (a) Edison type thermomagnetic prototype. (b) Detail of the Gd rotor placed at the magnetic circuit gap.

3.4 Heat sink and source

The prototype uses the cold water tank with adjustable temperature, as shown in Figure 5a, as a heat sink. The heat sink temperature is PID controlled using an N-type thermocouple inside the cold water. A Peltier element TEC1-12706 12V assembled with a water block heat exchanger was used to maintain the heat sink temperature constant during the tests.

A graphite thermal block was used as a heat source, as shown in Figure 5b. The heat source temperature was PID controlled by a 12V PTC heater using an N-type thermocouple as the temperature sensor. Figure 5c shows the heat sink and source placed at the prototype.

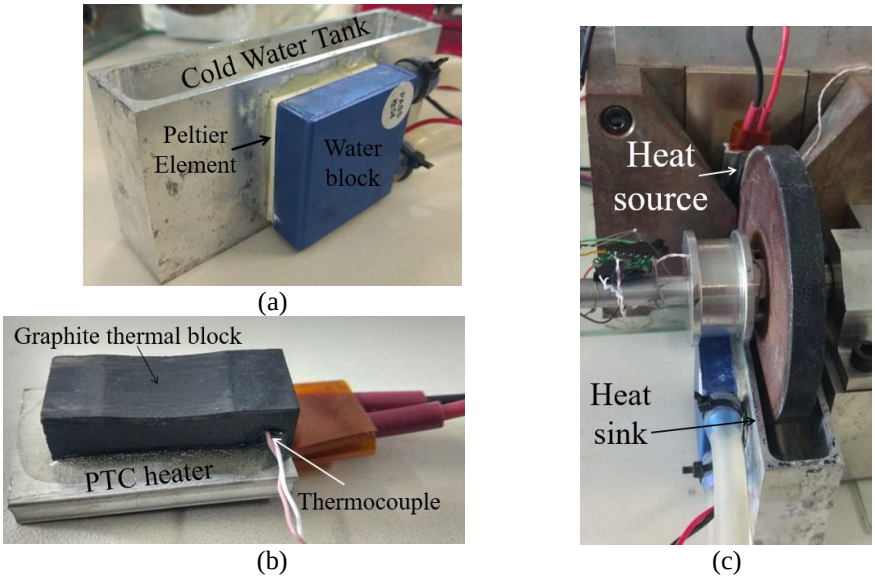

(a) (b) (c)

Figure 5. (a) Adjustable temperature heat sink. (b) Adjustable temperature heat source. (c) Heat sink and source placed at the thermomagnetic motor prototype.

4. EXPERIMENTAL PROCEDURE

The experimental procedures performed are described below.

4.1 Applied magnetic field profile

In order to determine the applied magnetic field distribution, the assembly shown in Figure 6 was used. The Gd rotor was removed from the shaft and replaced by a mounting with a Hall effect sensor CYSJ362A. The position of the

Hall effect sensor in relation to the stator was the same as the thermocouple mounted on the Gd rotor. The angular position α was determined by the angular encoder, so that when the Hall effect sensor was in the gap center α is 180º. The applied magnetic field was determined by turning the shaft a few times while collecting the data from the sensors.

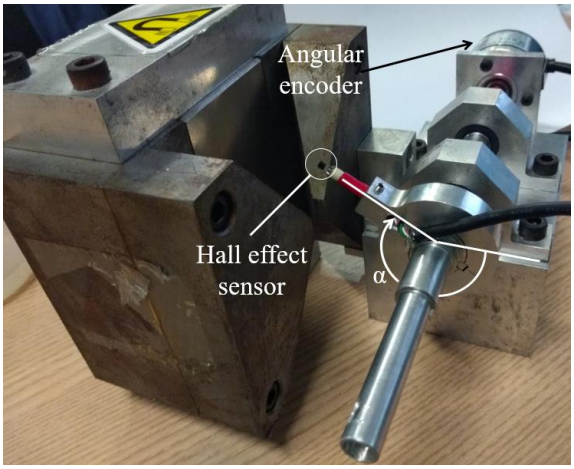

Figure 6. Applied magnetic field determination experiment.

4.2 Thermomagnetic motor power behavior

The power behavior of the prototype shown in Figure 4 was determined by using the assembly shown in Figure 7. First, the heat sink and source temperatures were set. Then, using lead weights, a torque was applied to the motor's shaft, and the torque was defined by multiplying the total lead weight in the basket by the pulley radius r. Next, the angular shaft velocity was determined by differentiating the angular position α with respect to time. When the system reaches the steady-state the data acquisition system registers the time, angular position, rotor temperature, and heat sink and source temperatures during three complete turns on the shaft. Next, the average power was calculated by multiplying the torque applied to the motor's shaft (τ) and the average angular velocity ω. After that, a new lead weight was added to the basket, applying a new torque to the shaft. This procedure was repeated considering different heat sink and source temperatures and applied shaft torques.

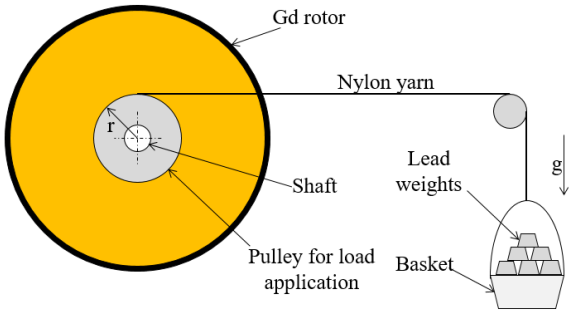

Figure 7. Experiment to determine the prototype power behavior.

5. RESULTS

5.1 Applied magnetic field profile

Figure 8 shows the magnetic field distribution provided by the thermomagnetic stator, the applied magnetic field changes from 0 up to 0.85 T, resulting in a high applied magnetic field gradient. The equation (1) can be used as a precise fit for the magnetic field distribution, having a root-mean-square deviation (R^2) of 0.9969, μ_0 is the vacuum magnetic permeability, x can be calculated by using equation (2), the parameters a, b and c are shown in Table 1 and W is an experimentally determined dimensionless constant which is valued as 0.55^{-1}.

$$\mu_0 H = a_1 e^{-\left(\frac{Wx-b_1}{c_1}\right)^2} + a_2 e^{-\left(\frac{Wx-b_2}{c_2}\right)^2} + a_3 e^{-\left(\frac{Wx-b_3}{c_3}\right)^2} + a_4 e^{-\left(\frac{Wx-b_4}{c_4}\right)^2} \quad (1)$$

$$x = \frac{\alpha - 180^o}{180^o} \tag{2}$$

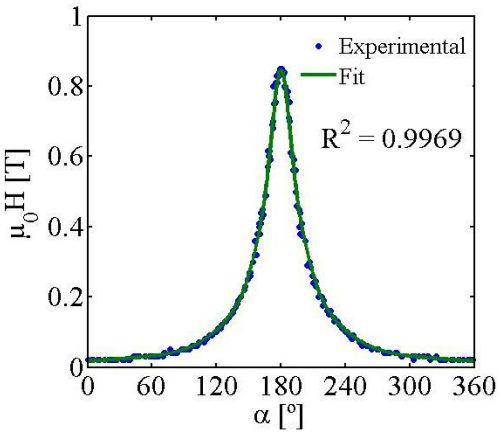

Figure 8 – Magnetic field distribution provided by the prototype stator.

Table 1. Magnetic applied field fit parameters.

Index	*a* [T]	*b* [-]	*c* [-]
1	0,3429	$-3{,}057\times10^{-5}$	0,2315
2	0,2498	$-8{,}771\times10^{-6}$	0,09805
3	0,2075	$-1{,}102\times10^{-5}$	0,5538
4	0,04736	$-4{,}608\times10^{-5}$	1,819

5.2 Thermomagnetic motor power behavior

Figure 9 shows the angular position as a function of the time by considering the heat sink temperature of 288 K and the heat source temperature of 298 K for three different applied torque conditions. As expected, the increase in the applied torque reduces the motor angular velocity for the same heat sink and source condition. In addition, one can note that the angular velocity suffers small oscillations by considering the same torque and heat sink and source conditions, possibly due to the stick-slip effect caused by the friction between the heat source and the Gd rotor. The results obtained for other torque and heat sink and source temperatures have similar profiles to those shown in Figure 9.

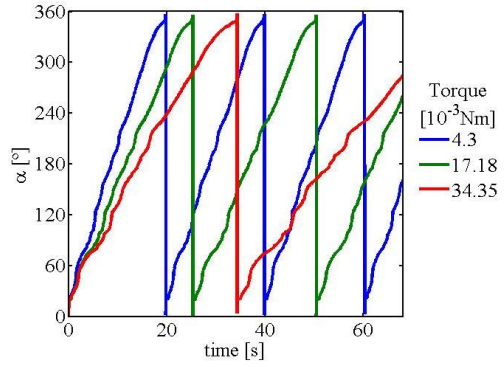

Figure 9. Angular position as a function of time by considering T_{Cold} = 288 K and T_{Hot} = 298 K and different shaft applied torques.

Figure 10 shows the behavior of the average angular velocity as a function of the applied torque by considering different heat sink and source temperatures. The results lead to the same conclusions obtained for Figure 9. The equation (3) is proposed as a fit for the angular velocity as a function of applied torque by considering the experimental data, ω is the average angular velocity in rad/s, and τ is the torque applied to the motor shaft in N.m. The parameters *k* and *m* are shown in Table 2.

$$\omega = ke^{-m.\tau} \tag{3}$$

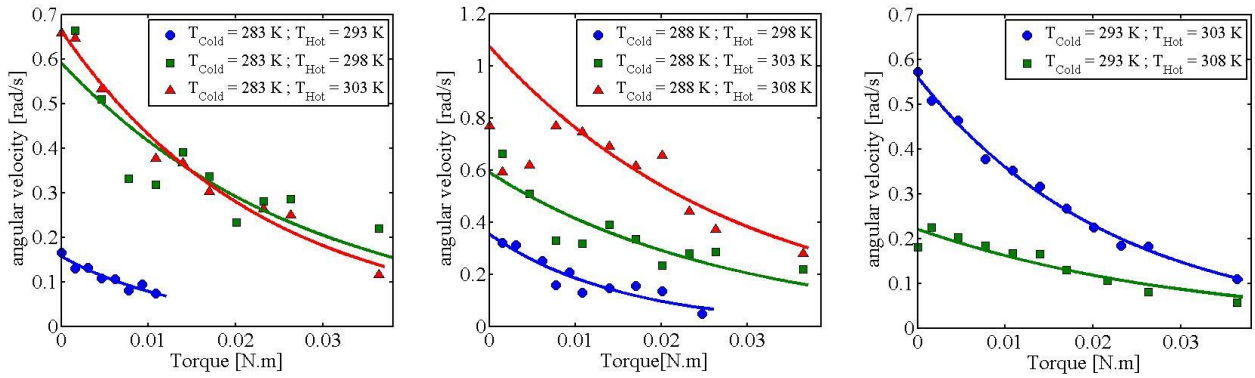

(a) (b) (c)

Figure 10. Angular velocity as a function of the applied shaft torque for: (a) T_{cold} = 283 K. (b) T_{cold} = 288 K. (a) T_{cold} = 293 K.

Table 2. Angular velocity as a function of applied shaft torque parameters and R^2.

T_{Cold} [K]	T_{Hot} [K]	k [rad/s]	m [m/N]	R^2
283	293	0,1571	70,3138	0,9224
283	298	0,5914	35,4625	0,7436
283	303	0,6633	43,3078	0,9825
288	298	0,3538	64,9498	0,8547
288	303	0,5914	35,4625	0,7436
288	308	1,0775	34,4985	0,8978
293	303	0,2201	31,1137	0,8789
293	308	0,5599	44,5660	0,9935

The average power P can be calculated using equation (4). Figure 11 shows the average mechanical power for the different heat sink and source temperature conditions and applied shaft torque. It is possible to note that the $P(\tau)$ presents a maximum point. The equation (5) was obtained by substituting (3) into (4), these profiles are similar to those experimentally obtained by Murakami & Nemoto (Murakami and Nemoto, 1972).

$$P = \omega.\tau \tag{4}$$

$$P = \tau k e^{-m.\tau} \tag{5}$$

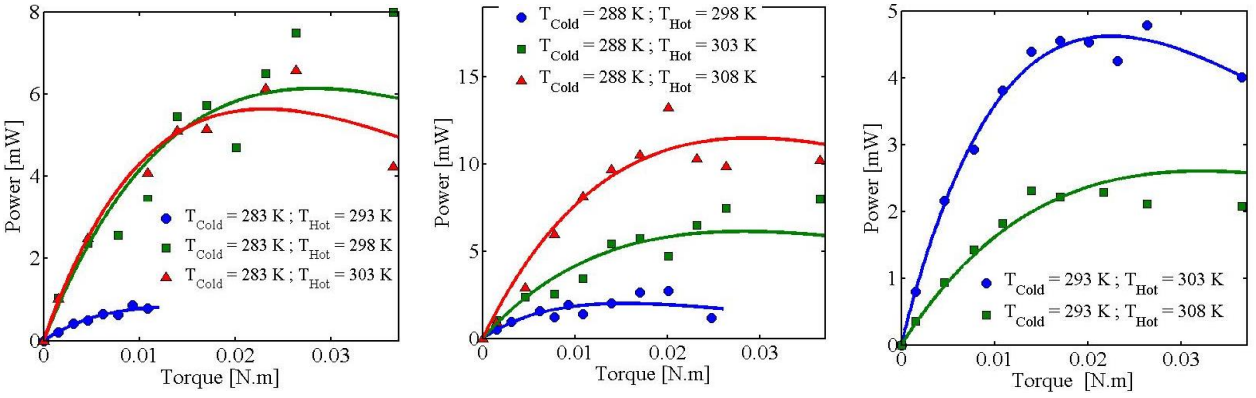

(a) (b) (c)

Figure 11. Mechanical average power as a function of the applied shaft torque for: (a) T_{cold} = 283 K. (b) T_{cold} = 288 K. (a) T_{cold} = 293 K.

6. CONCLUSIONS

An Edison type thermomagnetic motor prototype was built and tested, being able to produce a mechanical power of 12 mW for a heat sink and source temperature difference of only 20 K. It was also shown that the prototype could operate with temperature differences of only 10 K. A high applied magnetic field was obtained using a simple magnetic circuit with a large permanent magnet, the stator magnetic circuit can be replaced for a more complex but lighter magnet array. A higher power output could feasibly be obtained by increasing the size of the system, as in this test stand prototype the rotor contains only 32 g of magnetic material. The heat exchange can be easily improved by replacing the heat source for a hot water mass flow instead of the graphite thermal block. A set of experimental data was obtained and can be used to validate Edison type thermomagnetic motors mathematical models. A list of the main contributions of this study is shown below:

- Through an experimental approach, the relations of torque, angular velocity, and power were determined for an Edison type thermomagnetic motor prototype.
- Fits for the experimental data have been proposed, and they can easily be used to validate numerical models of these devices.
- A simple magnetic circuit capable of producing a strong applied magnetic field change of 0.85 T was built and tested.
- It was shown that the built prototype could produce useful work with a temperature difference of only 10 K.

7. ACKNOWLEDGEMENTS

This work was supported by Instituto Mauá de Tecnologia, IMT-SE-293/20. The authors would like to thank the Coordenação de Aperfeiçoamento de Pessoas de Nível Superior – Brasil (CAPES) – Finance Code 001 and Fundação de Amparo à Pesquisa do Estado de São Paulo – FAPESP (2019/06717-0).

8. REFERENCES

Ahmed, R., Park, J.C., Zeeshan, Mehmood, M.U., Lim, S.H., Lee, J., Chun, W., 2021. Optimization of a cylindrical thermomagnetic engine for power generation from low-temperature heat sources. Int. J. Energy Res. https://doi.org/10.1002/er.6396

Almanza, M., Pasko, A., Mazaleyrat, F., LoBue, M., 2017. First- Versus Second-Order Magnetocaloric Material for Thermomagnetic Energy Conversion. IEEE Trans. Magn. 53, 1–6. https://doi.org/10.1109/TMAG.2017.2697398

Alves, C.S., Colman, F.C., Foleiss, G.L., Vieira, G.T.F., Szpak, W., 2013. Numerical simulation and design of a thermomagnetic motor. Appl. Therm. Eng. 61, 616–622. https://doi.org/10.1016/j.applthermaleng.2013.07.053

Bessa, C.V.X., 2018. Métodos analíticos para o cálculo de desempenho de motores termomagnéticos do tipo Tesla. Universidade de São Paulo, São Paulo. https://doi.org/10.11606/T.3.2018.tde-04102018-133241

Bessa, C.V.X., Ferreira, L.D.R., Horikawa, O., Gama, S., 2018. On the relevance of temperature, applied magnetic field and demagnetizing factor on the performance of thermomagnetic motors. Appl. Therm. Eng. 145, 245–250. https://doi.org/10.1016/j.applthermaleng.2018.09.061

Edison, T.A., 1888. Pyromagnetic Motor. US Patent 380,100.

Egolf, P.W., Kitanovski, A., Diebold, M., Gonin, C., Vuarnoz, D., 2009. Magnetic power conversion with machines containing full or porous wheel heat exchangers. J. Magn. Magn. Mater. 321, 758–762. https://doi.org/10.1016/j.jmmm.2008.11.044

Ferreira, L.D.R., 2019. Development of a rotary thermomagnetic motor for thermal energy conversion. Universidade de São Paulo, São Paulo. https://doi.org/10.11606/T.3.2019.tde-06052019-150249

Ferreira, L.D.R., Bessa, C.V.X., da Silva, I., Gama, S., 2014. A heat transfer study aiming optimization of magnetic heat exchangers of thermomagnetic motors. Int. J. Refrig. 37, 209–214. https://doi.org/10.1016/j.ijrefrig.2013.09.010

Gama, S., Ferreira, L.D.R., Bessa, C.V.X., Horikawa, O., Coelho, A.A., Gandra, F.C., Araujo, R., Egolf, P.W., 2016. Analytic and Experimental Analysis of Magnetic Force Equations. IEEE Trans. Magn. 52, 1–4. https://doi.org/10.1109/TMAG.2016.2517127

Halbach, K., 1980. Design of permanent multipole magnets with oriented rare earth cobalt material. Nucl. Instruments Methods 169, 1–10. https://doi.org/10.1016/0029-554X(80)90094-4

Kaneko, G.H., Conceição, W.A.S., Clareth, F.C., Cocci, A.S., Alves, C.S., Pupim, G.C., Kubota, G.H., Oliveira, V.C., Trevizoli, P.V., 2020. Design and Experimental Evaluation of a Linear Thermomagnetic Motor Using Gadolinium: Preliminary Results. Appl. Therm. Eng. 186, 116472. https://doi.org/10.1016/j.applthermaleng.2020.116472

Karle, A., 2001. The thermomagnetic Curie-motor for the conversion of heat into mechanical energy. Int. J. Therm. Sci. 40, 834–842. https://doi.org/10.1016/S1290-0729(01)01270-4

Kishore, R.A., Singh, D., Sriramdas, R., Garcia, A.J., Sanghadasa, M., Priya, S., 2020. Linear thermomagnetic energy harvester for low-grade thermal energy harvesting. J. Appl. Phys. 127, 044501. https://doi.org/10.1063/1.5124312

Kohl, M., Gueltig, M., Wendler, F., 2018. Coupled Simulation of Thermomagnetic Energy Generation Based on NiMnGa Heusler Alloy Films. Shape Mem. Superelasticity. https://doi.org/10.1007/s40830-018-0148-1

Lima, L.F.A., Santos, M.U.L., Correa, L. dos S., Trevizoli, P. V., 2020. THERMODYNAMIC ANALYSIS OF THERMOMAGNETIC MOTORS, in: 18th Brazilian Congress of Thermal Sciences and Engineering. pp. ENCIT2020-0047. https://doi.org/10.26678/ABCM.ENCIT2020.CIT20-0047

Mehmood, M.U., Zeeshan, Kim, Y., Ahmed, R., Lee, J., Chun, W., 2021. Design and operation of a thermomagnetic engine for the exploitation of low-grade thermal energy. Int. J. Energy Res. er.6804. https://doi.org/10.1002/er.6804

Murakami, K., Nemoto, M., 1972. Some experiments and considerations on the behavior of thermomagnetic motors. IEEE Trans. Magn. 8, 387–389. https://doi.org/10.1109/TMAG.1972.1067406

Paganotti, A., Bessa, C.V.X., Silva, L.S., Silva, R.A.G., 2019. Metallic sample preparation for phase transformation analysis. MethodsX. https://doi.org/10.1016/j.mex.2019.09.041

Risser, M., Vasile, C., Keith, B., Engel, T., Muller, C., 2012. Construction of consistent magnetocaloric materials data for modelling magnetic refrigerators. Int. J. Refrig. 35, 459–467. https://doi.org/10.1016/j.ijrefrig.2011.11.001

Tesla, N., 1889. Thermo Magnetic Motor. US Patent 396,121.

Vuarnoz, D., Kitanovski, A., Gonin, C., Borgeaud, Y., Delessert, M., Meinen, M., Egolf, P.W., 2012. Quantitative feasibility study of magnetocaloric energy conversion utilizing industrial waste heat. Appl. Energy 100, 229–237. https://doi.org/10.1016/j.apenergy.2012.04.051

9. RESPONSIBILITY NOTICE

The authors are the only responsible for the printed material included in this paper.